Malaysian Journal of Chemistry, 2024, Vol. 26(5), 358-369
(Special Issue: *4th IKMPB Online Symposium 2024 - Development of Chemistry to Accomplish a Sustainable World*)

Photodegradation of Methylene Blue over WO_3/TiO_2 Composites under Low UV-C Irradiation and Scavenger Analysis

Nik Fatin Nabihah Atiqah Nik Ramli[1], Hamizah Mokhtar[1]*, Zul Adlan Mohd Hir[2,3]*, Hartini Ahmad Rafaie[4], Nur Ariesha Jamaluddin[5] and Dzulaikha Khairudin[5]

[1]Civil Engineering Studies, College of Engineering, Universiti Teknologi MARA Pahang Branch, 26400 Bandar Tun Abdul Razak Jengka, Pahang, Malaysia

[2]Faculty of Applied Sciences, Universiti Teknologi MARA Cawangan Pahang Branch, 26400 Bandar Tun Abdul Razak Jengka, Pahang, Malaysia

[3]Catalysis for Sustainable Water and Energy Nexus Research Group, School of Chemical Engineering, College of Engineering, Universiti Teknologi MARA, 40450 Shah Alam, Selangor, Malaysia

[4]Centre of Foundation Studies, Universiti Teknologi MARA, Selangor Branch, Dengkil Campus, 43800 Dengkil, Selangor, Malaysia

[5]School of Civil Engineering, College of Engineering, Universiti Teknologi MARA Shah Alam, 40450 Shah Alam, Selangor, Malaysia

*Corresponding author (e-mail: hamizah1161@uitm.edu.my; zuladlan@uitm.edu.my)

The wastewater from the textile industry comprises a wide variety of dyes and chemicals, which makes wastewater disposal environmentally problematic. In particular, prolonged exposure to Methylene Blue (MB) dye has been shown to present significant dangers, particularly to human endocrine and environmental systems. The most effective technique for successfully removing contamination is to use heterogeneous semiconductor oxides as photocatalysts, which rely on the presence of reactive radical species and can function at ambient temperatures and pressures. Thus, the primary goals of the current study are to prepare and characterize WO_3/TiO_2 composite photocatalysts, as well as to test the photocatalytic activity against MB under low-intensity UV-C irradiation (9W). The mass ratio of WO_3 varies from 0.1 to 0.4 g using a facile mixing method. The SEM-EDX analysis indicates that the composites exhibit an irregular spherical shape, and the elements are homogeneously distributed corresponding to WO_3/TiO_2 photocatalyst. The functional group of the composite shows wider intensities at 483, 814, and 998 cm^{-1}. Meanwhile, the structural properties of the composite photocatalysts show the attribute of triclinic and orthorhombic crystal systems for WO_3 and TiO_2, respectively. The photocatalytic activity of the composite is higher than that of pure WO_3 and TiO_2. The WO_3/TiO_2 with a ratio of 0.3:0.1 (WT3), displaying a rapid and almost complete photocatalytic degradation (98.71%) within 180 min under UV-C irradiation, under normal conditions (10 mg/L, 25°C). Based on a pseudo-first-order kinetic model, the maximum degradation rate constant of 2.65 10^{-3} min^{-1} is obtained when h^+ and •OH are the primary active species during the process. Overall, this study highlights the substantial prospect for the implementation of composite photocatalysts in extensive wastewater treatment systems.

Keywords: TiO_2; methylene blue; photocatalyst; water treatment; WO_3

Received: January 2024; Accepted: July 2024

The production of textiles, papers, and leather has long involved the use of organic dyes in the textile industry, which produces a significant amount of contaminated water [1]. To meet the growing demand for water in industry, agriculture, and other domestic activities, wastewater should be treated for reuse. Conventional water treatment methods such as ultrafiltration, sludge, reverse osmosis, and adsorption are ineffective for the degradation of dyes due to their intricate molecular structure and high stability, making them difficult to remove. Moreover, the treatment using these physical methods only transferred the organic compound to a different phase and resulted in secondary pollution [2–4]. The secondary pollutants that are produced need post-treatment, which adds to the expense of solid waste management and time-consuming [5, 6]. Alternatively, heterogeneous semiconductor photocatalysis has been proposed to treat the polluted water. This approach has been regarded as a promising technique due to its viable, easy-to-implement, non-toxic, and inexpensive of eliminating pollutants from wastewater, particularly dyes [7–10].

Photocatalysis is the process by which a semiconducting material undergoes light-induced production of photogenerated charge carriers for degradation of organic pollutants in water. In order to

†Paper presented at the 4th IKMPB Online Symposium 2024 – Development of Chemistry to Accomplish a Sustainable World

treat the polluted water, light-harvesting semiconductor oxide materials that are non-toxic and environmentally friendly must be used [11]. Theoretically, when a semiconductor photocatalyst is exposed to light with the desired wavelength, it will absorb sufficient photons energy corresponding to its band gap. This phenomenon results in the excitation of electrons from the valence band (VB) to the conduction band (CB), creating electron-hole pairs (e^- and h^+) at the surface of the photocatalyst. Through a reductive process, the photogenerated electrons in the CB can generate superoxide radical anions ($\bullet O_2^-$), which have the reduction potential to break down the pollutant molecules. Meanwhile, the positive holes have a high oxidation potential, and they can react with hydroxide ions (OH^-) or water molecules to produce hydroxyl radicals (•OH), which are also involved in the degradation process.

In particular, an n-type semiconductor called tungsten trioxide (WO_3) has recently been identified as a promising photocatalyst to break down an assortment of organic pollutants in water [12]. Great UV/visible absorption, resistance to oxidation and acidity, low cost, low toxicity, strong chemical stability, and enhanced optical performance are some of this semiconductor's benefits. WO_3 has a broader range of applications, including water treatment which are supported by its electrical properties [13]. Nonetheless, pure WO_3 has some disadvantages which are a higher rate of charge carrier recombination and a low band gap energy, despite its capacity to react towards UV/visible light. Many researchers have put effort into suppressing the limitations by constructing composite materials through various approaches to enhance their physicochemical properties for practical applications. Interestingly, forming heterojunctions with other semiconductor metal oxides could overcome the problem and offer several benefits such as extensive light-absorption range, rapid mass transfer, and effective electron-hole separation efficiency [14]. By coupling WO_3 with different substances, its surface and electrical properties can be altered, simultaneously improving its photocatalytic performance.

Recently, titanium dioxide (TiO_2) has become more popular as a cost-effective, ecologically safe, photostable material for creating heterojunctions with WO_3. Its broad bandgap of 3.20 eV makes it a promising candidate for enhancing charge separation under UV. Based on previous studies, photocatalytic activity is further enhanced by the heterostructure formation and WO_3/TiO_2 synergistic interaction. Zhao et al. shows that, under simulated solar irradiation, charge carrier separation at the heterojunction interfaces caused charge transfer from the WO_3 to the TiO_2 surfaces to occur via heterojunction [15]. Similarly, mixing WO_3 and TiO_2 could yield a greater surface area and more surface-active sites than their counterpart alone [16, 17]. With the appropriate ratio and band alignment, it is possible to lower the charge recombination rate, which enhances high electron transport and boosts photocatalytic activity.

Therefore, in the present work, we provide a straightforward fabrication process for WO_3/TiO_2 composite photocatalysts using a simple chemical mixing approach. The amount of WO_3 was varied while the amount of TiO_2 remained constant to prepare several composites with various ratios. The WO_3/TiO_2 photocatalysts' morphology and surface composition were investigated using scanning electron microscopy (SEM) equipped with an energy dispersive X-ray (EDX) analyzer. X-ray Diffraction (XRD) and Fourier Transform Infrared (FTIR) were used to examine the structural and functional groups of the WO_3/TiO_2 composite photocatalysts, respectively. The photocatalytic performance was evaluated against Methylene Blue (MB) in an aqueous solution assisted by a low-intensity UV light (9 W) irradiation. Moreover, the effects of several parameters including the catalyst dosage and initial MB concentration were investigated. Additionally, the possible degradation mechanism of MB over WO_3/TiO_2 was also analyzed along with the identification of the major reactive species during the scavenger test. It is expected that the resultant heterojunction photocatalytic material provides insightful inspiration for the construction of highly efficient composite photocatalysts for the water treatment process.

EXPERIMENTAL

Chemicals and Materials

Tungstic acid ($H_2WO_4 \geq 99\%$), commercial titanium dioxide (TiO_2, 99%), and methylene blue ($C_{16}H_{18}N_3S^+ \geq 98\%$) were obtained from Sigma Aldrich (Selangor, Malaysia). Hydrogen peroxide (H_2O_2, 30-35%) was purchased from R&M Chemicals (Selangor, Malaysia). All chemicals have been used and applied as received and deionized water was used throughout the experimental procedures.

Preparation of WO_3

Approximately 2.5 g of tungstic acid ($H_2WO_4 \geq 99\%$) was dissolved in 100 mL of hydrogen peroxide with continuous stirring until a colorless solution was formed. Next, the solution was left to dry in the oven at 60°C for 2 hours to remove the remaining solvent. The dried yellowish powder was then collected and calcined in a muffle furnace at 500°C for 2 hours [18]. The powder was stored for later use.

Table 1. Compositions for the preparation of WO_3/TiO_2 composite photocatalysts.

WO_3 (g)	TiO_2 (g)	Photocatalyst
0.1	0.1	WT1(1:1)
0.2	0.1	WT2 (2:1)
0.3	0.1	WT3 (3:1)
0.4	0.1	WT4 (4:1)

Preparation of WO_3/TiO_2 Composite Photocatalyst

A facile chemical mixing method was used to prepare the WO_3/TiO_2 photocatalysts by varying WO_3 mass ratios [19, 20]. Firstly, 0.1 g of WO_3 and 0.1 g of commercial TiO_2 were mixed and dispersed in 100 mL of deionized water while being continuously stirred for 1 hour. The obtained pale-yellow sample was identified as WO_3:TiO_2 = 1:1 (WT1) after being dried overnight at 80°C in the oven. The WO_3/TiO_2 composite was prepared using the same process previously mentioned with other mass ratios of WO_3 to TiO_2 (2:1, 3:1 and 4:1). Pure WO_3 was also prepared without the addition of TiO_2 for comparison purpose. Table 1 shows the composition of the prepared photocatalysts.

Evaluation of Photocatalytic Performances

Methylene blue (MB) dye was subjected to photodegradation in an immersion well photoreactor. The calibration plot of the targeted pollutant, in an aqueous solution under standard conditions was carried out before the photocatalytic testing. The calibration curve was plotted in accordance with the different targeted pollutant concentrations, which ranged from 5 to 25 mg/L. The linear equation was determined by measuring the absorbance of every sample at the maximum wavelength (λ_{max}= 665 nm) based on the calibration plot. A 250 mL glass photoreactor was used to test the photocatalytic activity of MB in an aqueous solution. A 9 W UV-C light was used as a light source. The photoreactor containing 100 mL of the working solution at a known concentration was filled with 0.2 g of the powder photocatalyst. In order to ensure that there was dissolved oxygen in the solution, the photoreactor was continuously supplied with air at a fixed flow rate of 4 L/min. The photoreactor was then subsequently permitted to remain in the dark for 30 minutes before initiating the photodegradation testing to reach adsorption-desorption equilibrium. After that, the photoreactor was exposed to irradiation from the UV light. At predetermined intervals, the sample of 5 mL was collected and filtered to separate the photocatalyst. The remaining MB concentration was determined using a UV-vis spectrophotometer (PerkinElmer Lambda 35). The following equation was used to estimate the degradation percentage.

$$Degradation\ percentage\ (\%) = \frac{(C_O - C_t)}{C_O} \times 100\% \quad (1)$$

Where C_O is the concentration of MB before irradiation and C_t is the concentration of MB at time 't'.

Kinetic Study

The Langmuir-Hinshelwood (L-H) kinetic model can be used to analyze a heterogenous photocatalytic reaction as shown:

$$r = -\frac{dC}{dt} = k_{obs}C \quad (2)$$

Equation (2) was integrated to produce a typical pseudo first-order equation as obtained:

$$ln\frac{C_O}{C} = k_{obs}C \quad (3)$$

where k_{obs} is the apparent pseudo first-order rate constant, C is MB concentration in the solution at a given irradiation time, t and C_O is initial MB concentration.

Characterization Methods

By using the Attenuated Total Reflection (ATR) Pellet technique, the functional groups of the prepared samples were examined using Fourier Transform Infrared (FTIR) analysis on a Perkin Elmer infrared spectrometer that covered a range of 450 cm^{-1} to 4000 cm^{-1}. X-ray powder diffractometer (XRD, PANalytical X'PERT-Pro MPD) was used at a scanning speed of 5°/min, Cu Kα1 radiation (λ = 1.540 Å, 45kV and 40mA) in the 2θ range of 10-90° to determine the sample's crystallinity degree and phases. Scanning electron microscope (SEM-EDX, TESCAN VEGA3) equipped with an electron-dispersive X-ray analyzer was also used to characterize the morphological and elemental compositions of the prepared photocatalysts.

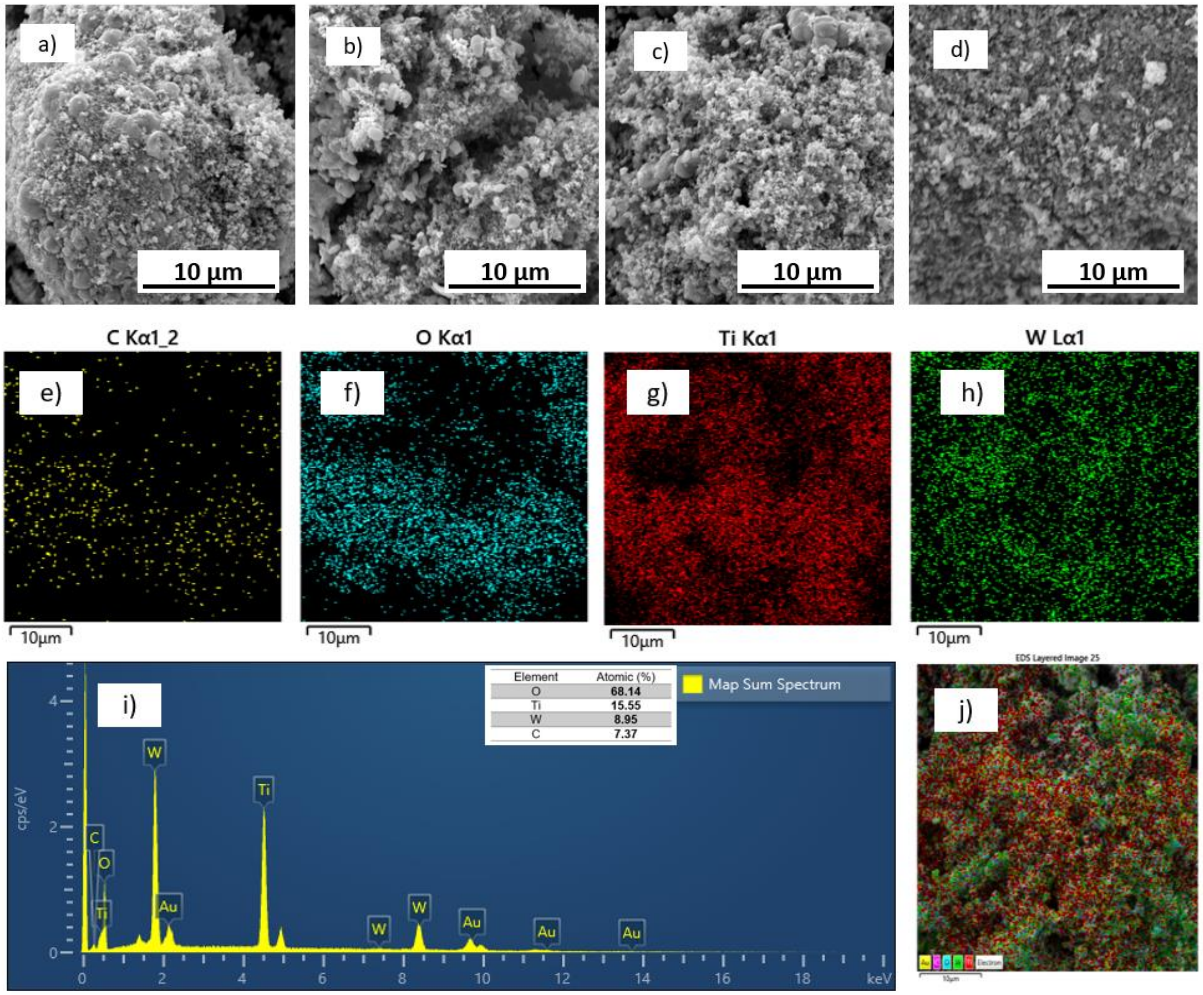

Figure 1. SEM images of (a) WO_3/TiO_2 (1:1), (b) WO_3/TiO_2 (2:1) (c) WO_3/TiO_2 (3:1) (d) WO_3/TiO_2 (4:1) composite photocatalysts at 3kx magnification and EDX analysis of the WO_3/TiO_2 (3:1) composite photocatalysts with corresponding elemental mapping images for (e) C, (f) O, (g) Ti, (h) W and (i) the elemental spectra and sample's composition

RESULTS AND DISCUSSION

Characterization

Scanning Electron Microscopy with Energy Dispersive X-ray Analysis (SEM-EDX)

Scanning electron microscopy (SEM) was used to examine each photocatalyst's morphological features. On the surface of the composite photocatalyst, elemental information has also been assigned by using energy dispersive X-ray analysis (EDX). The morphological surface of photocatalysts prepared with varying mass ratios (WO_3/TiO_2) is displayed in Figure 1. The images were captured at a magnification of 3000x. It is evident that all prepared composite photocatalysts of WO_3/TiO_2 exhibit similar irregular spherical shapes (Figure 1a-d) and the particles are seen to be evenly distributed on the surface. Nonetheless, the presence of individual WO_3 and TiO_2 are not clearly shown in the micrographs as there are some aggregations that have happened. There is also no significant difference in terms of the shape and morphology of the composite photocatalysts. Furthermore, the addition of TiO_2 appears not to affect the morphology of WO_3. The elemental composition of the WO_3/TiO_2 (3:1) composite is displayed in Figure 1(e-h). It can be seen that the particles have good dispersion as shown in the mapping images which are represented by the colors blue for O, red for Ti, and green for W. The composition is dominated by element O with an atomic percentage of 68.14%, followed by Ti (15.55%) and W (8.95%) (Figure 1i). The purity of the samples is confirmed by lack of additional peaks in the EDX pattern's and the Au peak's represents the gold coating used for the SEM images.

Fourier Transform Infrared Spectroscopy (FTIR) Analysis

In order to obtain a better understanding of the functional groups and chemical bond states of the

composite photocatalysts, FTIR technique was employed for characterization in Figure 2. In the FTIR spectra, the absorption peak values for pure WO_3 and pure TiO_2 are not shown in the results. However, the absorption of the composite material are similar to those of pure TiO_2, indicating that the addition of pure WO_3 does not change its chemical composition as stated in research by Priya et al., (2020) [21]. As shown in Figure 2, the intensity of the WO_3/TiO_2 composite obtained from the characterization that has been carried out in this research is roughly at 483 cm^{-1} and 814 cm^{-1} to 998 cm^{-1} [22, 23]. Thus, this causes the overlapping of the absorption peaks. By taking into consideration that the added WO_3 content is relatively low compared to the content of TiO_2 although a higher initial amount of dosage by WO_3 was added, the intensity of the wider absorption spectrum in the region of 450 to 1000 cm^{-1} has been reduced.

X-ray Diffraction (XRD) Analysis

A photocatalyst may exhibit a crystalline or amorphous structure. However, the degree of crystallinity greatly influences its reaction mechanism and overall activity. The crystalline phases have sharp melting points, faces and edges that reflect X-rays [24]. Figure 3 displays the XRD patterns of the WO_3/TiO_2 composite photocatalysts. The anatase TiO_2 pattern has several peaks, including the strongest peak of the (110) lattice planes, which is identified at 25.43º. The peak at 37.51º locates the (021) lattice plane. Meanwhile, the typical diffraction peaks of triclinic WO_3 are found at 23.16º, 24.34º, 27.17º, 28.85º, and 49.88º, with corresponding crystal indices of (002), (200), (201), (112), and (400). These crystal indices are referred from JCPDS card 071-0305 for WO_3 and JCPDS card 064-0863 for orthorhombic TiO_2. All of prepared composite photocatalyst samples show corresponding diffraction peaks for anatase TiO_2 and WO_3. As the WO_3 content was raised to 0.5g, the diffraction peaks of WO_3 became more apparent. The two-phase compositions of WO_3 and TiO_2 are readily visible in the WT1, WT2, WT3, and WT4 composite, as evidenced by their diffraction peaks and the lack of further peaks. When comparing all composite photocatalysts, the characteristic peaks' positions frequently don't change. This demonstrates that the stability of the lattice structures of their individual performance is unaffected by the WO_3/TiO_2 combination [25].

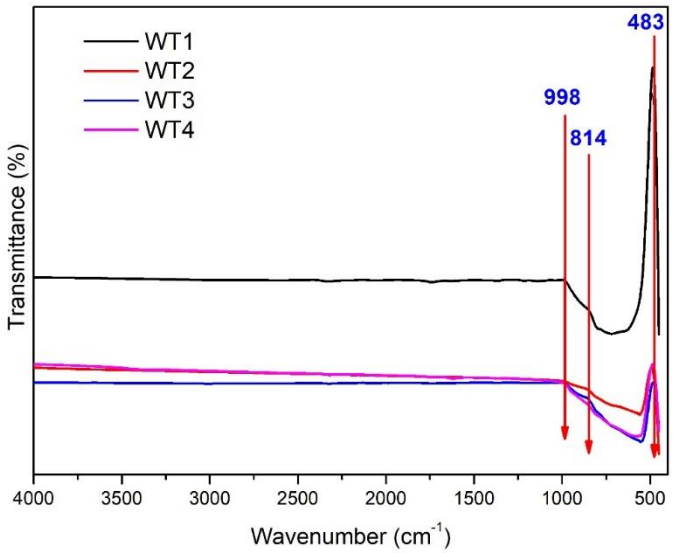

Figure 2. FTIR spectra of WO_3/TiO_2 composite photocatalysts with different mass ratios.

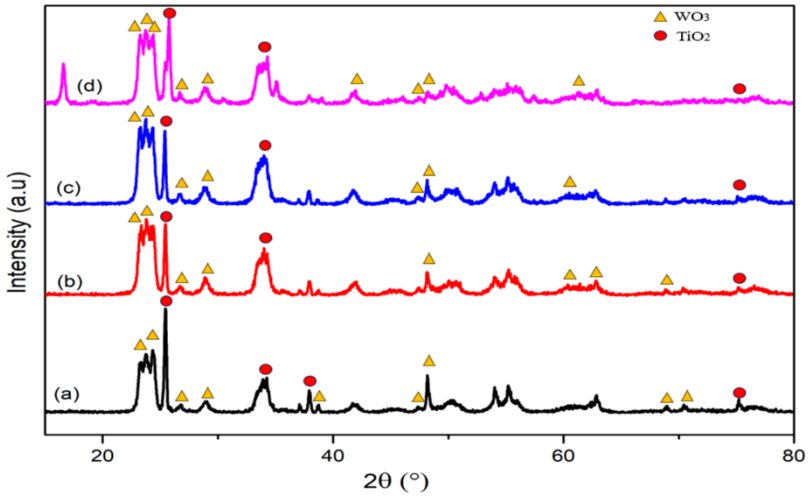

Figure 3. XRD pattern of (a) WO3/TiO2 (1:1), (b) WO3/TiO2 (2:1), (c) WO3/TiO2 (3:1), and (d) WO3/TiO2 (4:1) composite photocatalysts with different mass ratios.

Photocatalytic Performances Evaluation

The photocatalytic performances of all prepared photocatalysts were evaluated based on their capacity to degrade Methylene Blue (MB) when exposed to UV-C light. Over the course of 180 minutes, the percentage of MB degradation was plotted as a function of time (Figure 4). As demonstrated in Figure 4a, 14.02% of MB is degraded in the absence of a photocatalyst (photolysis) and this value appears to be insignificant. According to MB's direct photolysis, the molecule was remarkably stable and would not break down in the absence of a photocatalyst [26, 27]. In Figure 4b, the percentages of pure WO_3 and TiO_2 that show significant degradation are 95.93% and 94.21%, respectively. This demonstrates pure WO_3 and TiO_2 exhibit semiconductor qualities that can be used, upon exposure to UV light. However, the degradation percentage shows significantly lower values when two composite photocatalysts are combined at 1:1 (WT1) and 2:1 (WT2) ratio. Remarkably, at a ratio of 3:1 (WT4) in which the best composite photocatalyst shows the maximum degradation percentage of 98.71%. However, the photocatalytic performances decreased to 98.18% and 95.93% for 2:1 and 1:1 ratio, respectively when the mass of WO_3 was increased up to 0.4g. In theory, when photocatalysts are exposed towards light irradiation (photons) with energy equal to or much higher than their specific band gap, they are stimulated to produce photoinduced electrons (e^-) and positive holes (h^+) in the CB and VB [11].

Adsorbed oxygen and water then undergoes a series of redox reactions with those charge carriers which resulting in the formation of additional reactive radical species known as hydroxyl radicals (•OH) and superoxide radical anions ($•O_2^-$) [28]. The MB molecules that are on the photocatalyst surface will then be susceptible to attack by these reactive radical species. It will consequently mineralize the pollutants into such a harmless species, such as molecules of carbon dioxide and water. When combined with the best mass ratio, the optimal WT4 photocatalyst may result in a respectable heterojunction between WO_3 and TiO_2. By trapping the photoinduced electrons, the heterojunction formation can simultaneously increase the photocatalytic activity and decrease electron-hole recombination [29]. Furthermore, extending energy range of the photoexcitation may have increased charge separation which may account for the higher photocatalytic activity of the WT3 photocatalyst. Their unique physicochemical characteristics following significant modification may also have played an important role in this enhancement. However, the lower degradation percentages of WT1, WT2 and WT4 are caused by the quick recombination of photoinduced electron and hole pairs on the catalyst surfaces. This is consistent with another study that also shows the usage of WO_3/TiO_2 binary photocatalyst [30]. In order to form a potential composite photocatalyst with exemplary heterojunction formation, the synergistic interaction between WO_3 and TiO_2 is examined while taking into consideration their optimum mass ratio.

Upon aligning with irradiation light, the heterogeneous composite is able to absorb photons, consisting of excited electrons from the valence band towards the conduction band creating the electron-hole pairs. The WO_3/TiO_2 heterogeneous photocatalysts will take the opportunity to transfer the electron from WO_3 to TiO_2 in order to suppress the recombination. Migrated electrons can react with the adsorbed oxygen in order to generate the reactive oxygen species (ROS) or even participate in the reduction reactions. The photogenerated holes will directly oxidize the MB molecules adsorbed on the catalyst surface.

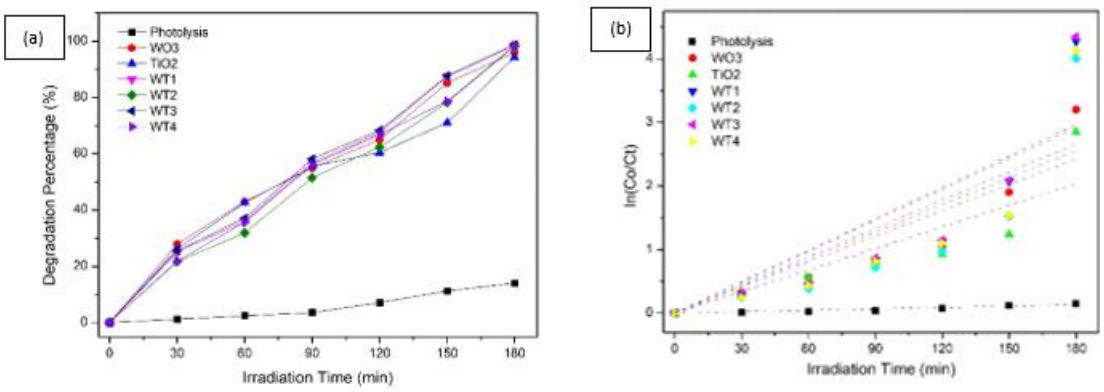

Figure 4. (a) Degradation percentage of MB in aqueous by using pure WO_3, pure TiO_2 and WO_3/TiO_2 composite photocatalysts with different mass ratios and (b) Kinetic data for degradation of MB in aqueous solution by using pure WO_3, pure TiO_2 and WO_3/TiO_2 composite photocatalysts with different mass ratios. [MB] = 10 mg/L, pH = 7, catalyst loading = 0.2 g

The pseudo-first-order model at low concentrations serves as an example of the Langmuir-Hinshelwood model, which is the most commonly used model of evaluating the kinetics study of photocatalytic systems [31–33]. The photocatalytic disintegration of MB, the pollutant is regulated by pseudo-first-order kinetics. Figure 4(b), Figure 5(b) and Figure 6(b) show the corresponding linear graph. The linear plots were used to calculate each photocatalyst's rate constant. The data exhibit a linear relationship with R^2 being closest to 1 in the pseudo-first-order kinetic model [34]. The results are in line with a study in Figure 4(b), Figure 5(b), Figure 6(b) and Table 2, Table 3, and Table 4 that discovered pure WO_3, pure TiO_2 and WO_3/TiO_2 composite photocatalysts establish first-order kinetics for the photocatalytic degradation of MB.

Based on Table 2, the correlation coefficient between the degradation percentage and the kinetic data for all the photocatalysts are high in which ranging from 0.84221 for WT1 to 0.9845 for photolysis process. This strong correlation coefficient indicates that the kinetic model provides such a very excellent fit in describing the photocatalytic degradation process for all different photocatalysts. In other words, the degradation rate constant can be used to effectively predict the expected degradation percentage of the pollutant. Thus, the most efficient photocatalyst for degradation of methylene blue appears to be WT3 with the 98.71% removal.

Photocatalyst Loading Effects

The photocatalysis process is significantly impacted by the photocatalyst dosage under UV-C irradiation when employing WT (3:1) composite photocatalyst. The degradation of MB was carried out using a dosage ranging from 0.1 to 0.5 g as shown in Figure 5. In this work, the best composite photocatalyst demonstrates the highest photocatalytic performance at 0.2 g dosage with a degradation percentage of 98.71%. This is explained by the fact that sufficient active sites are available to absorb enough photon energy from the exposure to UV-C light. It is clear that the availability of surface-active sites increases with the catalyst amount. Consequently, there are more reactive species ($\bullet OH$, $\bullet O_2^-$, h^+, e^-) that are in charge and responsible for degrading MB. The tendency of the particles to aggregate may also cause the degradation rate to slow down at some point. This would reduce the amount of surface-active sites and result in inefficient light absorption [35].

Table 2. Degradation percentage and kinetic data of all photocatalysts.

Photocatalyst	Degradation percentage (%)	K_{obs} (min^{-1})	Correlation factor, R^2
Photolysis	14.02	0.00006	0.94845
WO_3	95.93	0.00155	0.91411
TiO_2	94.21	0.00151	0.88703
WT1	98.61	0.00261	0.84221
WT2	98.18	0.00269	0.79271
WT3	98.71	0.00265	0.84355
WT4	98.39	0.00269	0.80686

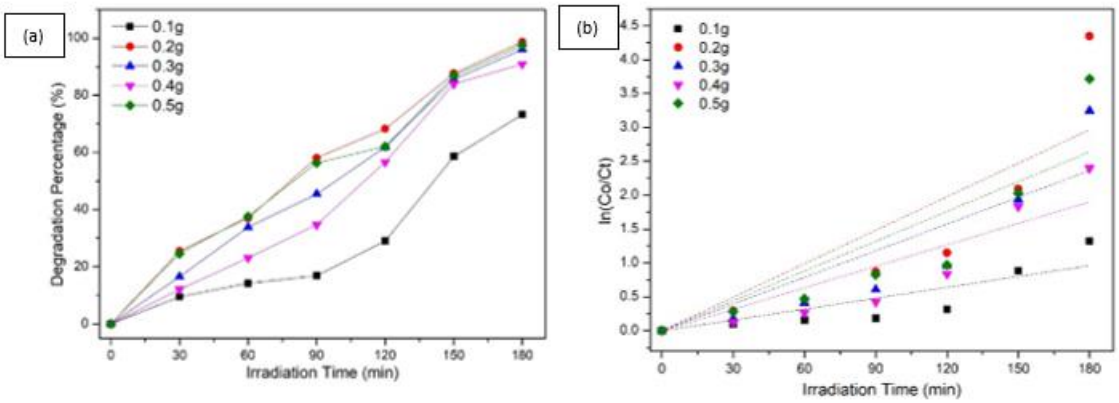

Figure 5. (a) Degradation percentage of MB in aqueous by using WO_3/TiO_2 (3:1) composite photocatalysts with different loading photocatalysts and (b) Kinetic data for degradation of MB in aqueous solution by using pure WO_3, pure TiO_2 and WO_3/TiO_2 composite photocatalysts with different photocatalysts loading. [MB] = 10 mg/L, pH = 7, catalyst loading = 0.1–0.5 g

Table 3. Degradation percentage and kinetic data of all photocatalysts with different photocatalysts loading.

Photocatalyst loading (g)	Degradation percentage (%)	K_{obs} (min^{-1})	Correlation factor, R^2
0.1	73.33	0.00860	0.84318
0.2	98.71	0.00265	0.84355
0.3	96.11	0.00185	0.87624
0.4	90.91	0.00139	0.89066
0.5	97.57	0.00214	0.86793

The data in Table 3 suggests a trend between the loading amount of photocatalyst and the degradation rate constant and the correlation coefficient. It is important to analyze the specific values in order to determine if K_{obs} increases or decreases with adjusting the amount of catalyst loading and if the correlation coefficient remains consistently high. A high correlation coefficient which ranges around 0.8 indicates that the chosen kinetic model provides such a good fit for the experimental data. This implies that the reaction rate can be well-predicted by the K_{obs} value for each photocatalyst loading. Thus, the 0.2 g loading photocatalyst records the highest percentage of degradation which is also chosen as the most efficient catalyst loading.

Initial Concentration Effects

The samples underwent analysis as indicated in Figure 6 in order to determine the percentage of degradation achieved for the initial MB concentration. These findings demonstrate how the photodegradation process's efficiency with the WT (3:1) catalyst is influenced by the concentration of MB. In general, the photocatalytic activity increases with decreasing initial MB concentrations. Previous research shows that the degradation efficiency dropped from 98.87% to 75.56% when the initial concentration of MB was increased from 5 to 25 mg/L. This may result from a greater concentration of pollutants occupying the catalyst's surface which leaves the catalyst's surface lacking active sites [36]. Moreover, it might be related to the intermediate by-products created during the process competing for the same catalysts' active sites. Alternatively, it might be the case that as the concentration of the solution increases, UV photons cannot penetrate the solution and their length of path becomes shorter [36].

Based on the data shown in Table 4, the degradation percentage and the kinetic data appear to exhibit a complex relationship. Meanwhile, the R^2 value obtained is relatively high with 0.84355 and 0.97797 for 10 and 20 ppm, respectively. The degradation rate is more sensitive towards the lowest initial concentration which is 5 ppm and becomes less dependent compared to higher concentrations which are 20–25 ppm. Further analysis has potentially considered the kinetic models and explored the mechanisms behind the observed behaviour achieved. Thus, 5 ppm shows the highest percentage of removal which is 98.87% compared to 25 ppm which records the lowest percentage of degradation which is 75.56%.

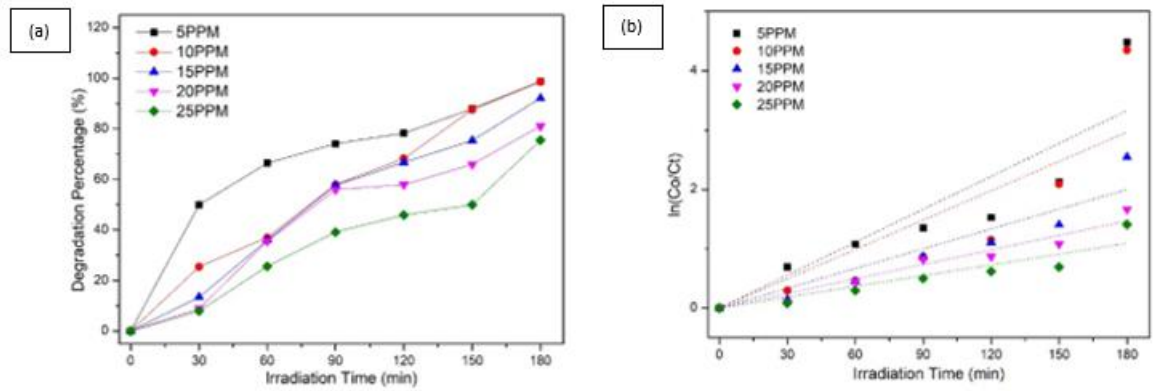

Figure 6. (a) Degradation percentage of MB in aqueous by using WO_3/TiO_2 (3:1) composite photocatalysts with different initial concentrations and (b) Kinetic data for degradation of MB in aqueous solution by using pure WO_3, pure TiO_2 and WO_3/TiO_2 composite photocatalysts with different initial concentration. [MB] = 5–25 mg/L, pH = 7, catalyst loading = 0.2 g

Table 4. Degradation percentage and kinetic data of all photocatalysts with different initial concentrations.

Initial concentration (ppm)	Degradation percentage (%)	K_{obs} (min^{-1})	Correlation factor, R^2
5	98.87	0.00219	0.90939
10	98.71	0.00265	0.84355
15	92.14	0.00103	0.94291
20	81.08	0.00046	0.97797
25	75.56	0.00059	0.93527

Radical Scavengers Test

The photocatalysis process is significantly impacted by the radical scavenger test under UV-C irradiation when employing WT (3:1) composite photocatalyst. The degradation of MB was carried out by applying three different reagents namely, p-benzoquinone, 1-propanol, and EDTA to scavenge the superoxide radical anions ($\bullet O_2^-$), hydroxyl radicals (•OH), and positive holes (h^+), respectively, as shown in Figure 7. In this work, 10 mL of 0.1 M of each scavenging agent was added into 100 mL of 10 mg/L MB aqueous solution. From the results obtained, p-benzoquinone resulted in the highest degradation percentage of 93.33%. This can be explained by the fact that there may be a small amount of $\bullet O_2^-$ species in the MB working solution. Meanwhile, 1-propanol manages to scavenge the presence of •OH since the degradation percentage obtained is 78.71%. Interestingly, the addition of EDTA produces the lowest degradation percentage of about 56.11% (Figure 7a). All in all, this means that the presence of h^+ is the major active species responsible for the degradation of MB in aqueous solution, followed by •OH and $\bullet O_2^-$. Figure 7b shows the kinetic disappearance of MB by using these three radical scavengers and the degradation percentage as well as the kinetic data are tabulated in Table 5.

Based on the data in Table 5, the photocatalytic degradation of MB appears to be influenced by the type of scavenger reagents used. The correlation coefficient values for all the reagents are relatively high which all exceed 0.9. This indicates that the graph consists of a good fit between the chosen kinetic model (pseudo first-order) and the experimental data. However, the degradation rate constant values varied depending on the scavenger. The presence of 1-propanol leads to the highest K_{obs} which is 0.0071 min^{-1}, suggesting the rapid scavenging of •OH radicals during the photodegradation process. Conversely, EDTA and p-benzoquinone seem to have less impact on the degradation rate with much lower K_{obs} of 0.0039 and 0.0011 min^{-1}, respectively, implying that the scavenging processes of the h^+ and $\bullet O_2^-$ species are much slower than that of 1-propanol. Overall, this test can also provide insights into the reaction mechanism for the MB degradation process over the WO_3/TiO_2 composite photocatalyst.

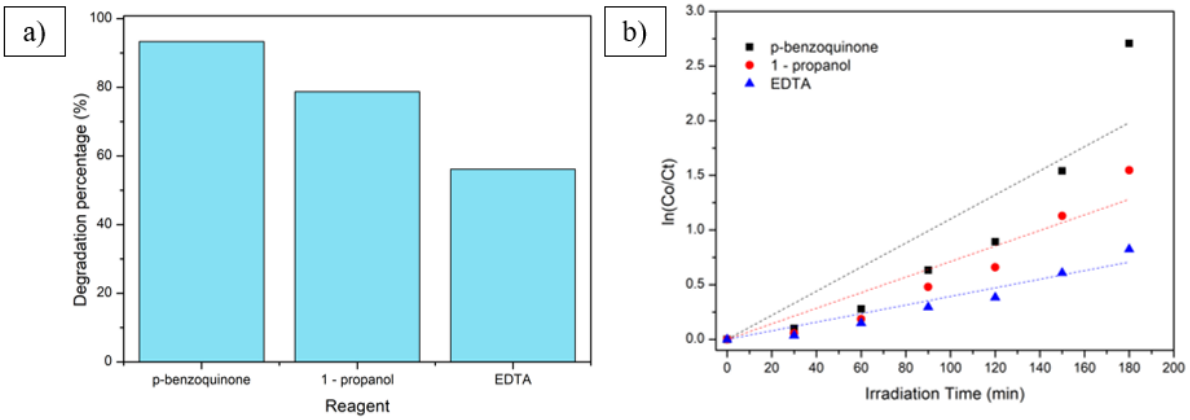

Figure 7. (a) Degradation percentage of MB in aqueous by using WO_3/TiO_2 (3:1) composite photocatalysts with different reagents for radical scavengers' test and (b) Kinetic data for degradation of MB in aqueous solution by using p-benzoquinone, 1-propanol, and EDTA reagent for radical scavengers' test. [MB] = 10 mg/L, catalyst loading = 0.2 g

Table 5. Degradation percentage and kinetic data of different types of reagents for scavengers' test

Reagent	Degradation percentage (%)	K_{obs} (min^{-1})	Correlation factor, R^2
p-benzoquinone	93.33	0.0011	0.9045
1-propanol	78.71	0.0071	0.9495
EDTA	56.11	0.0039	0.9697

CONCLUSION

A simple facile chemical mixing technique was used to successfully prepare WO_3/TiO_2 composite photocatalysts, with different mass ratios of each oxide. All of the prepared composites exhibited similar irregular spherical shapes, and the elements were homogeneously distributed corresponding to WO_3/TiO_2 photocatalyst. The functional group analysis showed the presence of WO_3 and TiO_2 in the structure. Meanwhile, the structural properties of the composite photocatalysts displayed the attribute of triclinic and orthorhombic crystal systems for WO_3 and TiO_2, respectively. From the photocatalytic results obtained, 0.2 g of WO_3/TiO_2 (3:1) composite showed the highest degradation percentage of 98.71% and this was chosen as the best photocatalyst in this study. The well-dispersed and synergistic interaction between WO_3 and TiO_2 photocatalyst promoted the efficient charge separation of the photogenerated electron-hole pairs and the ease of electron migration. These factors contributed to the enhanced photodegradation of MB in aqueous solution, under normal conditions. The initial concentration of 5 ppm recorded the highest degradation percentage which of 98.87% with a rate constant of 0.00219 min^{-1}. Based on scavenger effect analysis, the active species for the WT3 photocatalyst were photogenerated holes (h^+) and the •OH radicals. Overall, the best composite photocatalyst was stable against low-intensity UVC irradiation and provided a great deal of their potential in the photocatalytic water remediation process.

ACKNOWLEDGEMENTS

This research was funded by Ministry of Higher Education, Malaysia under the Fundamental Research Grant Scheme (FRGS) (Project Number: FRGS/1/2022/TK08/UITM/02/17), and Universiti Teknologi MARA Malaysia under the UiTM Grant (600-RMC/GPM LPHD 5/3 (166/2021). Authors also would like to thank Universiti Teknologi MARA (UiTM) Pahang Branch and UiTM Shah Alam for providing the services and facilities to carry out the laboratory work.

REFERENCES

1. Shivatharsiny, Y., Peng, R. & Koodali, R. (2015) An insight into the adsorption and photocatalytic degradation of rhodamine B in periodic mesoporous materials. *Applied Catalysis B Environmental*, **174-175**, 49–59.

2. Aboua, K. N., Yobouet, Y. A., Yao, K. B., Goné, D. L. & Trokourey, A. (2015) Investigation of dye adsorption onto activated carbon from the shells of Macoré fruit. *Journal of Environmental Management*, **156**, 10–14.

3. Bouazizi, A., Breida, M., Achiou, B., Ouammou, M., Calvo, J. I., Aaddane, A. & Younssi, S. A. (2017) Removal of dyes by a new nano-TiO_2/ ultrafiltration membrane deposited on low-cost support prepared from natural Moroccan bentonite. *Applied Clay Science*, **149**, 127–135.

4. Sahinkaya, E., Sahin, A., Yurtsever, A. & Kitis, M. (2018) Concentrate minimization and water recovery enhancement using pellet precipitator in a reverse osmosis process treating textile wastewater. *Journal of Environmental Management*, **222**, 420–427.

5. Gupta, A., Khosla, N., Govindasamy, V., Saini, A., Annapurna, K. & Dhakate, S. R. (2020) Trimetallic composite nanofibers for antibacterial and photocatalytic dye degradation of mixed dye water. *Applied Nanoscience (Switzerland)*, **10(11)**, 4191–4205.

6. Mousa, H. M., Alenezi, J. F., Mohamed, I. M. A., Yasin, A. S., Hashem, A. F. M. & Abdal-hay, A. (2021) Synthesis of TiO_2@ZnO heterojunction for dye photodegradation and wastewater treatment. *Journal of Alloys and Compounds*, **886**, 161169-161181.

7. Awasthi, G., Adhikari, S., Ko, S. W., Kim, H., Park, C. & Kim, C. (2016) Facile synthesis of ZnO flowers modified graphene like MoS_2 sheets for enhanced visible-light-driven photocatalytic activity and antibacterial properties. *Journal of Alloys and Compounds*, **682**, 208–215.

8. Fang, S., Lv, K., Li, Q., Ye, H., Du, D. & Li, M. (2015) Effect of Acid on the Photocatalytic Degradation of Rhodamine B over g-C_3N_4. *Applied Surface Science*, **358(a)**, 336–342.

9. Zhang, Z., Zhai, S., Wang, M., Ji, H., He, L., Ye, C., Wang, C., Fang, S. & Zhang, H. (2015) Photocatalytic degradation of rhodamine B by using a nanocomposite of cuprous oxide, three-dimensional reduced graphene oxide, and nanochitosan prepared via one-pot synthesis. *Journal of Alloys and Compounds*, **659**, 101–111.

10. Mariam, A., Elayaperumal, M., Kennedy, J., Ladchumananandasivam, R., Gomes, U. & Maaza, M. (2016) Solution processing of CuSe quantum dots: Photocatalytic activity under RhB for UV and visible-light solar irradiation. *Materials Science and Engineering: B*, **210,** 1–-9.

11. Mukhair, H., Abdullah, A. H., Hir, Z. A. M., Osman, N. S., Zainal, Z. & Hong Ngee, L. (2023) In-depth investigation on the photostability and charge separation mechanism of Ag_3PO_4/g-C_3N_4 photocatalyst towards very low visible light intensity. *Journal of Molecular Liquids*, **376**, 121494-121508.

12. Kubacka, A., Caudillo-Flores, U., Barba-Nieto, I. & Fernández-García, M. (2021) Towards full-spectrum photocatalysis: Successful approaches and materials. *Applied Catalysis A: General*, **610**, 117966–118051.

13. Ghanbari Shohany, B. & Khorsand Zak, A. (2020) Doped ZnO nanostructures with selected elements - Structural, morphology and optical properties: A review. *Ceramics International*, **46(5)**, 5507–5520.

14. Hir, Z. A. M., Mokhtar, H., Rafaie, H. A., Daud, S., Shohaimi, N. A. M. & Alam, N. M. F. H. N. (2024) Efficient photodegradation of paracetamol by TiO_2/ZnO photocatalyst and prediction via Fuzzy Inference System. *Iranian Journal of Catalysis (IJC)*, **14(2)**, 1–12.

15. Zhao, Q., Chen, S., Ren, B., Liu, S., Zhang, Y. & Luo, X. (2023) Fabrication and photocatalytic performance of WO_3/TiO_2 heterojunction composites. *Optical Materials*, **135**, 113266-113273.

16. Moghni, N., Boutoumi, H., Khalaf, H., Makaoui, N. & Colon, G. (2022) Enhanced photocatalytic activity of TiO_2/WO_3 nanocomposite from sonochemical-microwave assisted synthesis for the photodegradation of ciprofloxacin and oxytetracycline antibiotics under UV and sunlight. *Journal of Photochemistry & Photobiology, A: Chemistry*, **428**, 113848–113860.

17. Zhang, Y., Liu, D., Xiong, B., Li, J., Li, Y., Zhou, Y., Yang, A. -S. & Zhang, Q. -P. (2022) Constructing WO_3/TiO_2 heterojunction with solvothermal-sintering for enhanced photocatalytic activity under visible light irradiation. *Solid State Sciences*, **53**, 163–168.

18. Hir, Z. A. M. & Ali, R. (2021) Photodegradation of benzene, toluene, p -xylene in aqueous phase using ZnO, TiO_2, SnO_2, WO_3 and Fe_2O_3. *GADING Journal of Science and Technology*, **4(1)**, 25–32.

19. Cui, L., Ding, X., Wang, Y., Shi, H., Huang, L., Zuo, Y. & Kang, S. (2017) Facile preparation of Z-scheme WO_3/g-C_3N_4 composite photocatalyst with enhanced photocatalytic performance under visible light. *Applied Surface Science*, **391**, 202–210.

20. Zhao, Z., Ma, H., Feng, M., Li, Z., Cao, D. & Guo, Z. (2019) In situ preparation of WO_3/g-C_3N_4 composite and its enhanced photocatalytic ability, a comparative study on the preparation methods of chemical composite and mechanical mixing. *Engineered Science*, **7**, 52–58.

21. Priya, A., Senthil, R. A., Selvi, A., Arunachalam, P., Senthil Kumar, C. K., Madhavan, J., Boddula, R., Pothu, R. & Al-Mayouf, A. M. (2020) A study of photocatalytic and photoelectrochemical activity of as-synthesized $WO_3/g\text{-}C_3N_4$ composite photocatalysts for AO_7 degradation. *Materials Science for Energy Technologies*, **3**, 43–50.

22. Fan, G. (2020) Double photoelectron-transfer mechanism in $Ag{-}AgCl/WO_3/g\text{-}C_3N_4$ photocatalyst with enhanced visible-light photocatalytic activity for trimethoprim degradation. *Journal Hazard Material*, **403**, 123964–123970.

23. Smrithi, S. P., Kottam, N., Arpitha, V., Narula, A., A. G. N. and Subramanian K. R. V. (2020) Tungsten oxide modified with carbon nanodots: Integrating adsorptive and photocatalytic functionalities for water remediation. *Journal Science Advance Material Devices*, **5(1)**, 73–83.

24. Shandilya, P., Sambyal, S., Sharma, R., Mandyal, P. & Fang, B. (2022) Properties, optimized morphologies, and advanced strategies for photocatalytic applications of WO_3 based photocatalysts. *Journal of Hazardous Materials*, **428**, 128218–128253.

25. Medvedeva, E. D., Kozlov, D. A., Revenko, A. O. & Garshev, A. V. (2023) Synthesis of $g\text{-}C_3N_4/WO_3$ Composites under Hydrothermal Conditions and Study of Their Photocatalytic Properties, *†*. **14(1)**, 17–23.

26. Vione, D., Caringella, R., De Laurentiis, E., Pazzi, M. & Minero, C. (2013) Phototransformation of the sunlight filter benzophenone-3 (2-hydroxy-4-methoxybenzophenone) under conditions relevant to surface waters. *Science of the Total Environment*, **463–464**, 243–251.

27. Celeiro, M., Facorro, R., Dagnac, T., Vilar, V. J. P. & Llompart, M. (2019) Photodegradation behaviour of multiclass ultraviolet filters in the aquatic environment: Removal strategies and photoproduct identification by liquid chromatography–high resolution mass spectrometry. *Journal of Chromatography A.*, **1596**, 8–19.

28. Abdullah, R. R., Shabeed, K. M., Alzubaydi, A. B. & Alsalhy, Q. F. (2022) Novel photocatalytic polyether sulphone ultrafiltration (UF) membrane reinforced with oxygen-deficient Tungsten Oxide ($WO_{2.89}$) for Congo red dye removal. *Chemical Engineering Research and Design*, **177**, 526–540.

29. Shinde, D. R., Tambade, P. S., Chaskar, M. G. & Gadave, K. M. (2017) Photocatalytic degradation of dyes in water by analytical reagent grades ZnO, TiO_2 and SnO_2: a comparative study. *Drinking Water Engineering and Science*, **10**, 109–117.

30. Ruan, S., Huang, W., Zhao, M., Song, H. & Gao, Z. (2020) A Z-scheme mechanism of the novel ZnO/CuO n-n heterojunction for photocatalytic degradation of Acid Orange 7. *Materials Science in Semiconductor Processing*, **107**, 104835-104845.

31. Hossaini, H., Moussavi, G. & Farrokhi, M. (2017) Oxidation of diazinon in cns-ZnO/LED photocatalytic process : Catalyst preparation, photocatalytic examination, and toxicity bioassay of oxidation by-products. *Separation and Purification Technology*, **174**, 320–330.

32. Orooji, Y., Tanhaei, B., Ayati, A., Hamidi, S. & Alizadeh, M. (2021) Heterogeneous UV-Switchable Au nanoparticles decorated tungstophosphoric acid / TiO_2 for efficient photocatalytic degradation process. *Chemosphere*, **281**, 130795–130802.

33. Gong, C., Chen, F., Yang, Q., Luo, K., Yao, F., Wang, S., Wang, X., Wu, J., Li, X., Wang, D. & Zeng, G. (2017) Heterogeneous activation of peroxymonosulfate by Fe-Co layered doubled hydroxide for efficient catalytic degradation of Rhoadmine B. *Chemical Engineering Journal*, **321**, 222–232.

34. Pirsaheb, M., Hossaini, H., Asadi, A. & Jafari, Z. (2022) Enhanced degradation of diazinon with a $WO_3\text{-}Fe_3O_4/g\text{-}C_3N_4$-persulfate system under visible light (Pathway, intermediates toxicity and mechanism). *Process Safety and Environmental Protection*, **162**, 1107–1123.

35. Zhu, L., Li, H., Liu, Z., Xia, P., Xie, Y. & Xiong, D. (2018) Synthesis of the 0D/3D CuO/ZnO Heterojunction with Enhanced Photocatalytic Activity. *Journal of Physical Chemistry C.*, **122(17)**, 9531–9539

36. Imamović, B., Trebše, P., Omeragić, E., Bečić, E., Pečet, A. & Dedić, M. (2022) Stability and Removal of Benzophenone-Type UV Filters from Water Matrices by Advanced Oxidation Processes. *Molecules*, **27(6)**, 1874–1897.